




# Optics Letters

## Hypertelescope with multiplexed fields of view

ZONGLIANG XIE,<sup>1,2,3,4,7</sup>  THIERRY LEPINE,<sup>4,5</sup>  THOMAS HOULLIER,<sup>4,5,6</sup> HAOTONG MA,<sup>1,2,8</sup>  
DENIS MOURARD,<sup>3</sup> AND ANTOINE LABEYRIE<sup>3</sup>

<sup>1</sup>Key Laboratory of Optical Engineering, Institute of Optics and Electronics, Chinese Academy of Sciences, Chengdu 610209, China

<sup>2</sup>University of Chinese Academy of Sciences, Beijing 100039, China

<sup>3</sup>UCA/OCA/CNRS, Lab. Lagrange, 06108 Nice Cedex 2, France

<sup>4</sup>Univ-Lyon, Laboratoire Hubert Curien, UMR CNRS 5516, 18 rue Benoît Lauras, 42000 Saint-Etienne, France

<sup>5</sup>Institut d'Optique Graduate School, 18 rue Benoît Lauras, 42000 Saint-Etienne, France

<sup>6</sup>Sophia Engineering, 5 Rue Soutrane, 06560 Valbonne, France

<sup>7</sup>e-mail: zongliang.xie@yahoo.com

<sup>8</sup>e-mail: mahaotong@163.com

Received 13 December 2019; revised 3 February 2020; accepted 3 February 2020; posted 26 February 2020 (Doc. ID 385953); published 20 March 2020

**Hypertelescope interferometers having many highly diluted sub-apertures are capable of directly imaging, within a narrow field of view, celestial objects at a high resolution thanks to pupil densification. This Letter verifies with OpticStudio modeling the possibility of simultaneously imaging multiple such fields. A strategy of multi-field sampling uses a microlens array to generate multiplexed field channels, where independent active corrections of the tip-tilt and piston are applied for compensating for the off-axis aberrations. Adopting this strategy, we have designed a model of a multi-field hypertelescope with OpticStudio. The reported design expands the observing performance of hypertelescopes for directly imaging multiple sources with very high angular resolution.** © 2020 Optical Society of America

<https://doi.org/10.1364/OL.385953>

The idea of the hypertelescope proposed by Labeyrie [1] provides a potential solution, thanks to pupil densification with many highly diluted apertures, for producing resolved snapshot images of astrophysical objects. Over the past few decades, its special imaging properties, performance and limitations have been explored by different researchers [1–8]. A model derivation was performed by Aime [2] for better understanding the densification mode. Lardiere *et al.* [3] and Patru *et al.* [4] studied the properties of its field of view (FOV) and point spread function (PSF). Extensions of the basic theory have been proposed, including a speckle imaging mode [5], a co-phasing method [6], a deconvolution algorithm [7], and aperture pattern optimization [8].

Following the theoretical study with numerical simulations, laboratory experiments and actual sky testing with miniature versions have been performed on Vega [9] and Deneb [10], and the practical project of a Carlina hypertelescope, architected as a diluted version of the large Arecibo and FAST radio telescopes, has also been initiated [11].

Despite these inspiring developments, the hypertelescope principle initially appeared to have a major limitation: the small

direct imaging field (DIF) [3,4], compared to a Fizeau interferometer. Pupil densification providing the hypertelescope's direct imaging capability brings a sensitivity gain by transferring energy from the diffracted halo to the central interference peak, but also violates the “golden rule” of the Fizeau interferometer [12], thus restricting the field. Any interferometer has an intrinsic FOV limitation [3,4] called the clean field (CLF), the angular extent of which on the sky is simply expressed as  $CLF = \lambda/s$ , with  $\lambda$  being the imaging wavelength and  $s$  being the typical smallest baseline of the array. The CLF, corresponding to the angular extent of the clean central part of the PSF, is a consequence of the sampling theorem, irrespective of the beam combination method. A hypertelescope if fully densifying the pupil, however, provides a DIF equal to the CLF [1,3]. We discuss the further gain of field coverage achievable by creating on the sky a diluted multiple window providing an array of DIFs [13].

This Letter verifies through optical modeling with OpticStudio the multi-field concept proposed by the Refs. [13–15]. It divides a wide field into several sub-field channels, each equipped with independent phasing actuators. The off-axis aberrations can be corrected by adjusting tip-tilt and pistons within each off-axis field channel for interference-limited images of their stellar content. The proposed multi-field hypertelescope can be equivalently understood as an instrument composed of multiple independent hypertelescopes with differently tilted optical axes. They share some common optical components where their beams intersect, and each has its own corrected offset DIF, all providing adjacent images on a common camera sensor.

Pupil densification is performed by either magnifying each output sub-pupil or reducing the spacings. It concentrates the collected energy from the side lobes into the interference peak, thus increasing its intensity with respect to the Fizeau's beam-combining method. However, this significant improvement of sensitivity shrinks the DIF. The segmented wavefront from an on-axis point source is flat at the exit of the pupil densifier if suitably co-phased. If the source moves off-axis, the pupil

densification distorts the wavefront as a staircase [1], which causes a differential motion of the interference peak and the diffractive envelope in the focal image: the former moves faster, thus eventually reaching the edge of the envelope and becoming attenuated. This causes the field limitation, and implies the limited covered sky extent called the DIF [1].

Here the multi-field design is illustrated based on a Carlina hypertelescope, but is also applicable to telescope arrays. Among the opto-mechanical architectures considered for hypertelescopes, the “Carlina” type is an optical sparse version of giant radio telescopes such as Arecibo or FAST [11]. Unlike some conventional interferometers, it does not require optical delay lines and has a simplified optical train, favoring the use of hundreds or thousands of sub-apertures, which are foreseen to provide meta-apertures as large as 100,000 km when deployed in space [14]. As sketched in Fig. 1(a), such interferometers have a large concave primary meta-mirror M1 in sparse form, made of discrete segments which can be much smaller than their spacings, and a movable focal optical train suspended on the focal sphere. The beams that it receives from the observed star are co-focused as a Fizeau image at the entrance of the focal optics and then relayed through a pupil densifier onto the science camera.

The reflective segments of M1 can be simply arranged as a fixed spherical locus such as the Arecibo radio telescope. It then requires a corrector of spherical aberration in the optical train. Instead, if each M1 segment has micrometric actuators for tip-tilt and piston, the locus of the primary M1 can be actively shaped as a paraboloid as achieved at the FAST radio telescope in China. The active M1 segments can perform a sliding parabolic deformation such as a tsunami to keep the parabolic axis pointing toward the source during the celestial motion [11]. Such active paraboloid simplifies the focal train by eliminating the need for a spherical aberration corrector, while the coma correction for off-axis sources remains necessary.

In the Fizeau focal plane, a field lens L1 projects the sparse array of sub-pupils onto a dome-shaped pupil densifier, the elements of which are Galilean beam-expanders. Each contains a small negative lens L2 and a larger positive lens L3, magnifying the corresponding sub-pupil. A large beam-combining lens L4 co-focuses all beams into a combined image, further magnified by a small lens L5 onto the science camera.

The strategy of field multiplexing is used to address the DIF limitation. The model assumes an active paraboloidal M1 array, the curvature center of which is fixed, and the optical axis kept pointed toward the observed source. As mentioned above, only a small field around the optical axis is directly imaged with such a hypertelescope. Multiple optical axes provided by field sampling can be arranged by inserting

- (1) a microlens array L1a, replacing lens L1 in the Fizeau focal plane with angular pitch spacings on the sky exceeding about  $2\lambda/d$ , where  $d$  is the diameter of the M1 segment, to avoid the overlapping of neighbor diffractive envelopes in the Fizeau focal plane;
- (2) microlens arrays L2a replacing each L2 lens, making it possible to generate multiple DIFs;
- (3) a microlens array L5a replacing a single lens L5, for image magnification in each field channel.

The optical axes of all sub-fields are variously tilted relative to the main axis of the paraboloid. Each source’s primary image must be accurately centered in its sub-field window, for example, by using a small tiltable plate attached to each L1a lenslet. Without overlapping, such Fizeau spread functions can be separately fed to a pupil densifier to become hypertelescopic direct images, suitably arrayed on the common science camera. The overlap of adjacent sources is avoided if the source’s angular spacing exceeds the angular size of the sub-aperture’s diffraction envelope.

For each sub-aperture, within each densifier, wavefront corrections are thus needed for

- (1) accurately centering inside the corresponding DIF each source focused on the L1a microlens;
- (2) correcting the local co-phasing errors caused on its wavefront segment by coma for off-axis sources;
- (3) locally correcting residual co-phasing errors, including those induced by the atmospheric turbulence.

The focal optical train with multiplexed fields is sketched in Fig. 1(b). The green and red stars shown are focused on different L1a lenslets. Then the two sub-field beams are collected by L2a, which can be equipped with actuators for tip-tilt and piston, allowing independent co-phasing in each field channel, as needed for wavefront correction. Each L2a microlens array

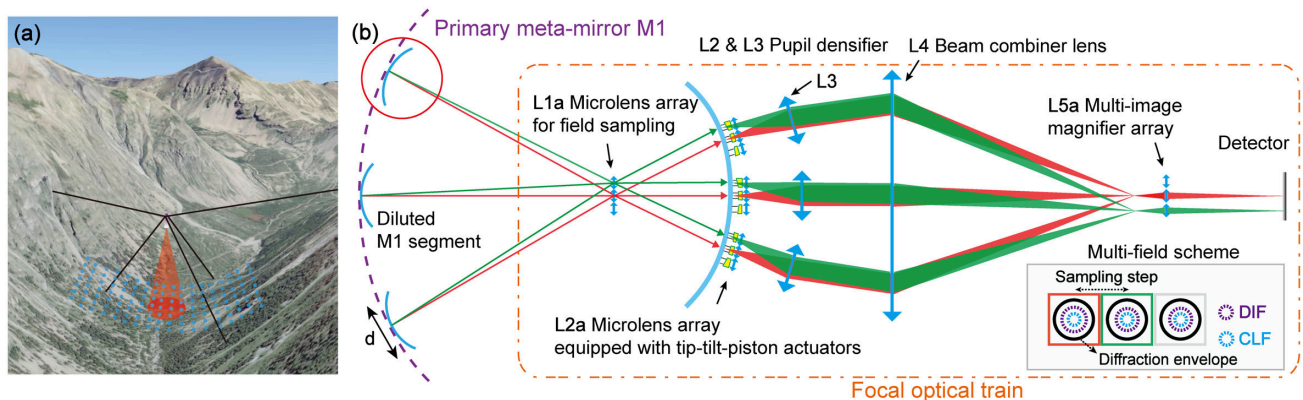


**Fig. 1.** Schematic of a Carlina hypertelescope with multiplexed field channels. (a) Diagrammatic Carlina hypertelescope and (b) focal optical train with field multiplexing (not a scale drawing). A microlens array L1a divides the field into several channels, each containing separate hypertelescopic images of different sources such as the green and red stars. L2a and L3 magnify each pupil in field channels, L4 co-focuses all beams, and L5a magnifies the images. As a result, multiple field channels are generated, each being usable for imaging a source smaller than the DIF size.

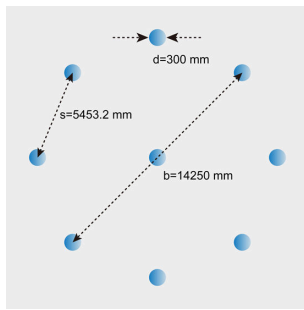


**Fig. 2.** Configuration of the segmented primary meta-mirror.

focuses on L3 a single combined and magnified image of the corresponding sub-pupil. L4 combines the beams from each source by co-phasing them as an array of separate sub-field images, matching the L1a pattern, but with wider gaps. As shown in the inserted box of Fig. 1(b), with off-axis aberrations corrected, a valid DIF is obtained within each of the field channels. Maximizing the densification, with sub-pupils then becoming adjacent, can minimize the DIF, then matching the usable CLF and maximizing the luminosity gain [3]. The multi-field channels can contain separate hypertelescopic images of different sources such as the green star and the close red one shown in Fig. 1(b). Finally, each L5a microlens magnifies the corresponding image for proper pixel sampling on the camera array. The gaps between the displayed images can also be reduced, for economy of camera pixels, by adjusting the spacings of the L5a microlenses.

To assess the effectiveness of the optical design, we modeled a Carlina hypertelescope with multiplexed fields in OpticStudio. It is scaled like the terrestrial prototype under test at Ubye in the southern Alps [11].

The M1 paraboloidal meta-mirror with curvature radius  $R_1 = 202$  m is sparsely segmented with nine elements much smaller than their spacings. The element diameter is 300 mm, and the wavelength is 550 nm. Figure 2 shows the aperture configuration. The minimum and maximum baselines are 5.45 and 14.25 m, respectively. For this configuration, the usable CLF is only 0.02 arcseconds around the axis.

Then a focal optical train shown in Fig. 3 is positioned on-axis at  $f_1 = R_1/2 = 101$  m above the nine sub-mirrors, a position called the “Fizeau focus,” where the primary images of the observed source are co-focused. For simplicity, all the lenses are ideally paraxial, the focal lengths of which are listed in Table 1. The diameter of the L1a lenslet in the model is chosen as 0.5 mm, corresponding to a sampling step of 1.008 arcseconds

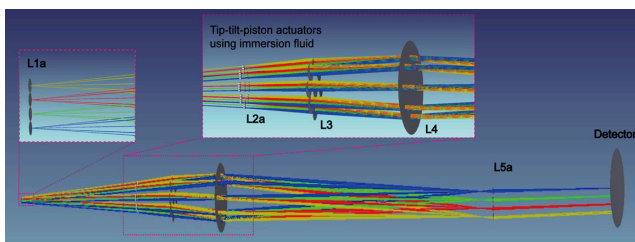


**Fig. 3.** Focal optical train with multiplexed field channels modeled in OpticStudio.

**Table 1.** Focal Optics Model Main Parameters

Optical Component	Focal Length
Microlens Array L1a	50 mm
Microlens Array L2a	−3 mm
Single Lens L3	25 mm
Single Lens L4	50 mm
Microlens Array L5a	5 mm

on the sky, about 2.6 times the size of the 0.38 arcsecond sub-aperture’s diffractive lobe, for a minimal cross-contamination of neighboring sources.

For multi-field imaging, it is important to make independent tip-tilt and piston adjustments available for each field channel, particularly for a terrestrial hypertelescope observing through the turbulent atmosphere. Then fast actuators and wavefront sensing are needed for adaptive phasing, and laser guide stars are necessary in the absence of bright natural stars [16,17]. Space versions of hypertelescopes with many sub-apertures will be much easier to control in terms of co-phasing and can use much fainter guide stars.

In the model, we propose a potential co-phasing actuator using tiltable window immersed on each L2a microlens, with three actuators providing tip-tilt-piston correction. Manipulating fluid to correct tip-tilt and pistons is realistic and promising in the future with the development of phase modulation techniques using electrowetting optofluidics [18].

Each of the microlens arrays L1a, L2a, and L5a contains four microlenses corresponding to the four respective field channels, centered at 0, 1.008, 2.016, and 3.024 arcseconds from the paraboloid’s optical axis, respectively. Within each field channel, a usable CLF of 0.02 arcseconds is expected.

Optical interferometric imaging, with the Fizeau or hypertelescope interferometers, requires that the diffractive envelopes from sub-apertures be superposed and the optical path differences be balanced. However, for off-axis fields, the coma of a paraboloidal meta-mirror violates both conditions. It decenters the spots from each M1 segment in the L5a focal plane in off-axis sub-fields, as shown in Fig. 4(a). The further from the axis, the more serious the aberration influence. Besides, the optical path lengths along the sub-aperture beams in off-axis channels also differ due to both the coma and pupil densification. The interference functions of all the sources, presented in Fig. 5(a), are calculated by the “Huygens PSF” tool

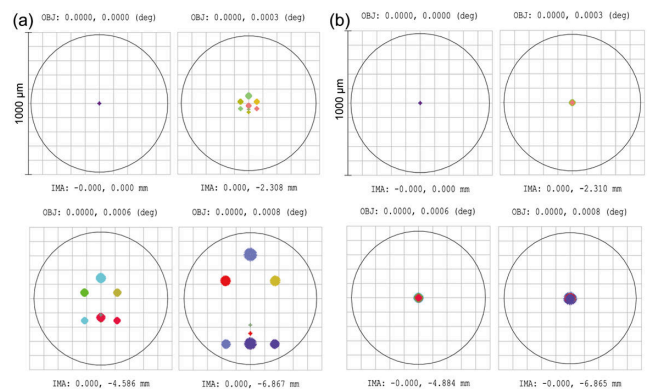


**Fig. 4.** Spot diagrams in the L5a focal plane of all the sub-field channels (a) without and (b) with corrections (different colors correspond to different segments).

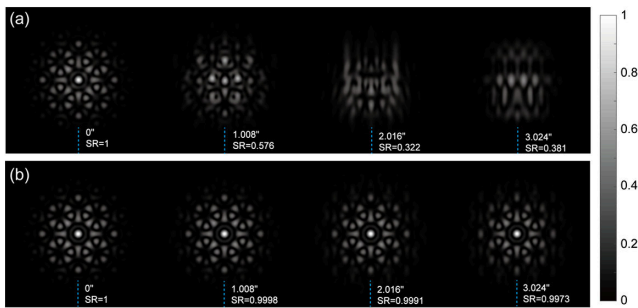


**Fig. 5.** PSFs in the L5a focal plane for sources centered in each sub-field channel (a) without and (b) with corrections. The theoretical angular resolution on the sky is 0.008 arcseconds.

in OpticStudio. As expected, there only appears a desired PSF with a dominant peak at the on-axis position, while at the off-axis positions the PSFs exhibit messy speckles. The Strehl ratio (SR) values of the PSFs of all the sources are 1, 0.576, 0.322, and 0.381.

Considering coma-induced aberrations as a composition of the tip-tilt and piston, we apply the co-phasing approach to correct coma. Within each of the off-axis field channels, the tip-tilt errors can be removed by superposing all the diffractive envelopes of sub-apertures, and the piston errors can be corrected by compensating for the optical path differences. Practical actuators proposed in Fig. 3 suffice per sub-field channel for independent tilt-tip and piston corrections. In practice, the tip-tilt and piston co-phasing can be driven by various wavefront sensing methods [6,19]. Here, for simplicity, we sense and adjust the errors by ray tracing in OpticStudio. Corresponding metrics are defined as spot position differences and optical path differences among all the sub-apertures in each off-axis field channel. The parameters of the co-phasing actuators immersed on each element of L2a, referring to tip-tilt-piston adjustments, are set as variables. Then the optimization in OpticStudio is performed to minimize the metrics to be zeros, generating the spot diagrams presented in Fig. 4(b). The amount of tilt correction for the actuator is within 0.8 deg, and the maximum piston needed to be compensated is 0.766 mm. As expected, in all sub-fields, the centroids of sub-aperture spots are well superposed with each other. We then test the property of the PSF for the center source of each channel. Figure 5(b) presents the results of imaging multiple sources centered in the four sampled field channels. The corrected results exhibit dominant central peaks containing most of the energy, implying that multiple CLFs are available. The PSFs of off-axis sources almost coincide with the on-axis one in terms of both the shapes and profiles. The corresponding SR values for the sources centered at 0, 1.008, 2.016, and 3.024 arcseconds on the sky are 1, 0.9998, 0.9991, and 0.9973, respectively. This confirms that the goal of simultaneously obtaining diffraction and interference-limited images of the multi-sources is reached.

This simulation of a rather modestly sized hypertelescope, having only a few sub-apertures and a small meta-aperture diameter, verifies the possibility of multi-field hypertelescope imaging. The optical design appears applicable to much larger versions, particularly in space with a meta-aperture, in the form of a mirror flotilla, containing many thousands of sub-apertures and spanning up to 100,000 km [14]. These instruments, in

principle, can show morphology details of an earth-like exoplanet at a few light years, with resolution matching the size of a large terrestrial city and a capability for detecting seasonal variations in spectro-images, as needed for searching evidence of photosynthetic life. For instance, a 100 km hypertelescope with a collecting area comparable to the E-ELT would directly image an exo-earth at 10 light years [13]. Globular clusters suspected as sites of life and intelligence may become efficiently observable with the multi-field arrangement since, some of their stars can be individually centered in each of the multi-field channels [13].

More work is needed to optimize the hypertelescope optics for multi-field imaging and other aspects such as exoplanetary coronagraphy. Theoretical modeling of off-axis aberration decomposition needs further study so as to give a quantified guide of compensating errors for practical designs. The off-axis aberrations are corrected via co-phasing using center sources of each field channel, inevitably leaving slight residual aberrations in the CLF. A global active coma corrector containing within each L2a array a conical elastic membrane could simultaneously correct all the coma-induced wavefront errors of all the sub-fields, which needs further exploration.

**Funding.** UCAS Joint PhD Training Program (UCAS[2015]37).

**Disclosures.** The authors declare no conflicts of interest.

## REFERENCES

1. A. Labeyrie, *Astron. Astrophys. Suppl. Ser.* **118**, 517 (1996).
2. C. Aime, *Astron. Astrophys.* **483**, 361 (2008).
3. O. Lardiere, F. Martinache, and F. Patru, *Mon. Not. R. Astron. Soc.* **375**, 977 (2007).
4. F. Patru, N. Tarmoul, D. Mourard, and O. Lardiere, *Mon. Not. R. Astron. Soc.* **395**, 2363 (2009).
5. A. Surya, S. K. Saha, and A. Labeyrie, *Mon. Not. R. Astron. Soc.* **443**, 852 (2014).
6. V. Borkowski, A. Labeyrie, F. Martinache, and D. Peterson, *Astron. Astrophys.* **429**, 747 (2005).
7. C. Aime, H. Lantéri, M. Diet, and A. Carlotti, *Astron. Astrophys.* **543**, A42 (2012).
8. F. Cassaing and L. M. Mugnier, *Opt. Lett.* **43**, 4655 (2018).
9. H. Le Coroller, J. Dejonghe, C. Arpesella, D. Vernet, and A. Labeyrie, *Astron. Astrophys.* **426**, 721 (2004).
10. H. Le Coroller, J. Dejonghe, F. Hespeels, L. Arnold, T. Andersen, P. Deram, D. Ricci, P. Berio, A. Blazit, J. M. Clause, C. Guillaume, J. P. Meunier, X. Regal, and R. Sottile, *Astron. Astrophys.* **573**, A117 (2015).
11. D. Mourard, A. Labeyrie, T. Lepine, P. D. Nunez, B. Tregon, and Z. Xie, *Exp. Astron.* **46**, 561 (2018).
12. W. A. Traub, *Appl. Opt.* **25**, 528 (1986).
13. A. Labeyrie, *EAS Publications Ser.* **78**, 45 (2016).
14. A. Labeyrie, *Handbook of Exoplanets* (2018), p. 168.
15. A. Labeyrie, L. Arnold, P. Riaud, O. Lardiere, V. Borkowski, S. Gillet, J. Dejonghe, and H. Le Coroller, in *European Southern Observatory Conference and Workshop Proceedings* (2002), Vol. **58**, p. 473.
16. P. D. Nuñez, A. Labeyrie, and P. Riaud, *Mon. Not. R. Astron. Soc.* **439**, 1787 (2014).
17. A. Labeyrie, *C. R. Physique* **8**, 426 (2007).
18. L. Li, H. Wang, Q. Wang, and S. Wu, *Opt. Express* **26**, 25839 (2018).
19. M. Deprez, C. Bellanger, L. Lombard, B. Wattellier, and J. Primot, *Opt. Lett.* **41**, 1078 (2016).